Atomic stick-slip friction as a two-dimensional thermally activated process

Quanzhou Yao [1,2] Jiawei Sun,[1] Xiaoying Zhuang,[2] Peter Wriggers,[3] Xi-Qiao Feng,[1,4] and Qunyang Li [1,4,*]

[1]*Applied Mechanics Laboratory, Department of Engineering Mechanics, Tsinghua University, Beijing, 100084, China*

[2]*Chair of Computational Science and Simulation Technology, Institute of Photonics, Department of Mathematics and Physics, Leibniz University Hannover, 30167 Hannover, Germany*

[3]*Institute for Continuum Mechanics, Leibniz University Hannover, Garbsen, Germany*

[4]*State Key Laboratory of Tribology, Tsinghua University, Beijing 100084, China*

(Received 9 September 2021; accepted 8 April 2022; published 25 April 2022)

Widely recognized as a thermally activated process, atomic stick-slip friction has been typically explained by Prandtl-Tomlinson model with thermal activation. Despite the limited success, theoretical predictions from the classic model are primarily based on a one-dimensional (1D) assumption, which is generally not compatible with real experiments that are two-dimensional (2D) in nature. In this letter, a theoretical model based on 2D transition state theory has been derived and confirmed to be able to capture the 2D slip kinetics in atomic-scale friction experiments on crystalline surface with a hexagonal energy landscape. Moreover, we propose a reduced scheme that enables extraction of intrinsic interfacial parameters from 2D experiments approximately using the traditional 1D model. The 2D model provides a theoretical tool for understanding the rich kinetics of atomic-scale friction or other phenomena involving higher dimensional transitions.

DOI: 10.1103/PhysRevB.105.165429

Since its first report on graphite [1], atomic stick-slip has been commonly observed in nanoscale friction experiments [2,3]. Its fundamental mechanism can be understood by Prandtl-Tomlinson model with thermal activation (PTT) [4–8], in which an independent oscillator is driven to move along a periodically corrugated energy landscape under thermal excitation. Although the PTT model can relate stick-slip behavior to intrinsic characteristics of the sliding interfaces, the statistical analyses [2,3,9–11] are derived predominantly based on one-dimensional (1D) assumption in contrast to the experiments that are essentially two-dimensional (2D) in nature. This disparity makes correct interpretation of experimental data prohibitively difficult, except in some idealized situations [3,11,12]. While physical differences between 1D and 2D models have been clarified by simulation [13], a better understanding of the 2D stick-slip behavior is imperative. In this work, we theoretically derive the slip probability in 2D force space, which is further validated by atomic-scale friction experiments. Based on the characteristics of the 2D slip force distribution, we propose a reduced slip force histogram that can be used to approximately extract the intrinsic interfacial parameters while still using the traditional 1D analysis.

To produce the 2D atomic stick-slip friction data used for subsequent theoretical modelling, we first performed numeric simulations by solving the 2D Langevin equations [14,15]

$$m\frac{d^2\mathbf{x}}{dt^2}+m\gamma\frac{d\mathbf{x}}{dt}+\frac{\partial V(\mathbf{x},\mathbf{s})}{\partial\mathbf{x}}=\xi(t), \tag{1}$$

where $\mathbf{x}=(x,y)$ is the position vector of the tip, V is the total potential energy including the tip-sample interaction U and the elastic energy of the spring, and ξ is a random force vector originating from thermal excitation (see the Supplemental Material [16] for details).

As schematically shown in Fig. 1(a), the tip scan direction is assumed to be different from the close-packed direction of the 2D energy landscape by a rotation angle θ to represent a generic sliding process. Here the hexagonal energy landscape is described by the following tip-sample interaction [11,14]:

$$U=-U_0\left[\cos\left(\frac{2\pi X}{a}\right)\cos\left(\frac{2\pi Y}{\sqrt{3}a}\right)+\frac{1}{2}\cos\left(\frac{4\pi Y}{\sqrt{3}a}\right)\right]. \tag{2}$$

Figures 1(b) and 1(c) show a typical set of in-plane force images and the corresponding line profiles for a simulation with $\theta=15^\circ$ (more results can be found in Fig. S1 of the Supplemental Material [16]). Using the modified line scan reconstruction (LSR) algorithm [11] (see Fig. S2 [16] for details), we identified the slip events as illustrated by the circles in Fig. 1(c). By counting the lateral forces of all slip events included in the data of Fig. 1(b) and Fig. S1 [16], we could plot the histograms of the lateral slip force f_x for the three systems, i.e., $\theta=0^\circ, 15^\circ, 30^\circ$. As indicated by Fig. 1(d), the histograms of the lateral slip force differ notably when the scan direction is varied, despite the fact that the interfacial parameters are actually identical. Further comparison demonstrates that none of the statistical distributions matches the theoretical prediction from the traditional 1D PTT [6,22,23] model (see Fig. S3 [16]). This inconsistency is primarily caused by the fact that the real effective energy

*To whom correspondence should be addressed: qunyang@tsinghua.edu.cn

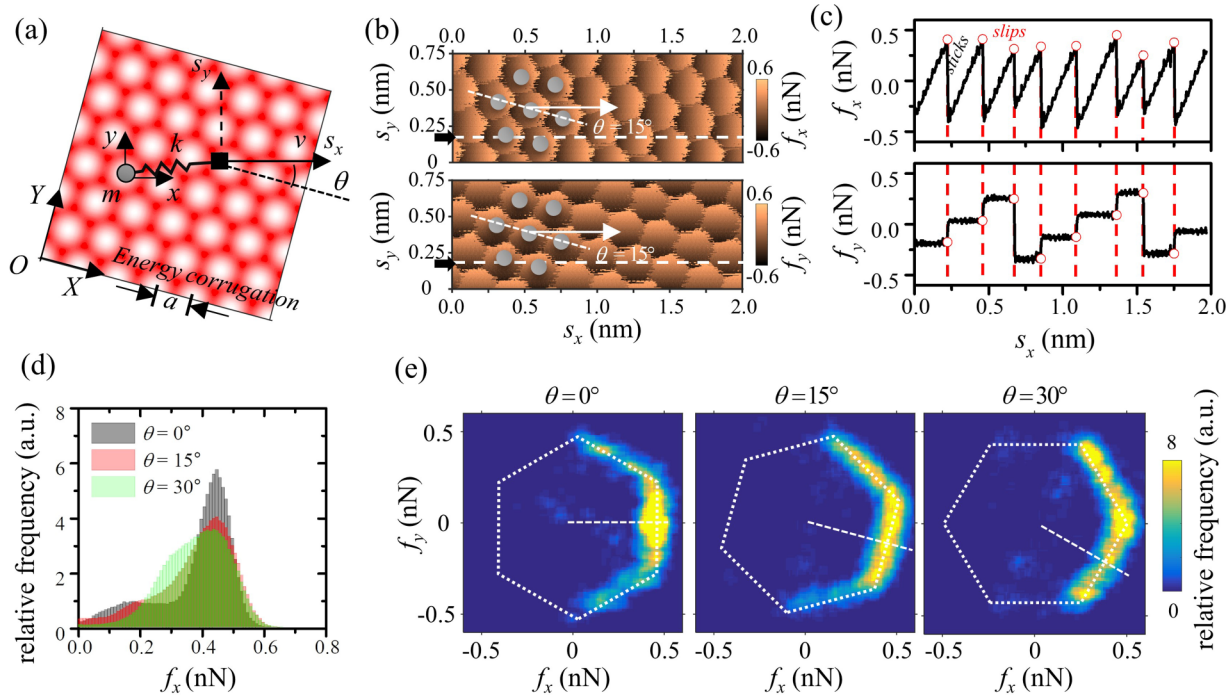

FIG. 1. (a) A schematic showing the simulation setup. (b) Lateral force f_x (upper panel) and axial force f_y (lower panel) images for $\theta = 15^\circ$. The gray dots visualize the periodic sites. (c) Lateral force f_x (upper panel) and axial force f_y (lower panel) traces for the white dashed lines marked in (b). The red circles indicate the extracted slip forces. (d) 1D histograms of the slip force f_x for $\theta = 0^\circ$ (black), $\theta = 15^\circ$ (red) and $\theta = 30^\circ$ (green). (e) 2D histogram of slip force for $\theta = 0^\circ$ (left), $\theta = 15^\circ$ (mid) and $\theta = 30^\circ$ (right). The dotted lines are visual guidelines to highlight the distribution shapes.

landscape experienced by the tip varies significantly when it slides along different paths on the 2D energy landscape [3]. In addition, the 2D zig-zag motion [12] also brings an extra complication to the slip process. Considering that the analysis of f_x in the traditional PTT model only provides 1D information, we speculate that supplementing it with the statistics of f_y may offer a more comprehensive description of the 2D slip behavior. Therefore, we plotted the 2D slip force histograms in Fig. 1(e) by counting the relative frequency of slip events in (f_x, f_y) space. In contrast to the irregular distributions shown in Fig. 1(d), the 2D histograms exhibit patterns with their shapes close to partial hexagonal annuluses. Moreover, the orientation of these patterns seems to change with the scan angle θ. This unique feature encourages us to develop a theoretical model to better understand the 2D slip behavior.

For a particle driven by a linear spring [24] on a 1D energy landscape without thermal activation, slip would occur [6,25] when the driving force reaches a critical value f_c (with a corresponding particle position, x_c) such that the local energy barrier vanishes. In the 2D scenario, since the particle can be driven along arbitrary directions on the 2D plane, the critical force becomes a vector set $\{\mathbf{f}_c\}$ in the force space. Meanwhile, each element in $\{\mathbf{f}_c\}$ has an associated critical slip position, $\mathbf{x}_c$, in the spatial coordinate space and an associated vector, $\mathbf{n}_s$, representing the corresponding direction along which the local energy barrier vanishes (see the Supplemental Material [16] for detailed derivations). The dashed curves in Figs. 2(a) and 2(b) show the sets of $\{\mathbf{x}_c\}$ and $\{\mathbf{f}_c\}$ in the spatial coordinate space and the force space, respectively, for the same energy landscape $V(\mathbf{x}, \mathbf{s})$ used in Fig. 1 with $\theta = 15^\circ$.

At finite temperature T, slip can occur with a transition rate, κ, even before the driving force $\mathbf{f}$ reaches its criticality due to thermal activation. Sang *et al.* [6] found that κ could be described by the Kramers' rate [20]:

$$\kappa = \frac{\Omega^2}{2\pi\gamma} \exp\left(-\Delta V / k_B T\right), \tag{3}$$

where ΔV is the transient energy barrier and Ω is the effective oscillation frequency. Since both ΔV and Ω vary as the particle is driven forward, they are functions of $\mathbf{f}$ [6,19,25,26]. Considering a particle that is driven to a nearly slip state, the transient force $\mathbf{f}$ would lie in the neighborhood of the critical set $\{\mathbf{f}_c\}$ in the force space. Because slip would likely occur along the direction with the smallest energy barrier, i.e., along the direction of $\mathbf{n}_s$, the corresponding energy barrier ΔV can be derived as follows:

$$\Delta V = \frac{4\sqrt{2}}{3}\left[-\mathbf{n}_s\mathbf{n}_s\mathbf{n}_s \vdots \nabla\nabla\nabla U(\mathbf{x}_c)\right]^{-1/2} \times \left[\mathbf{n}_s \cdot (\mathbf{I} + \lambda) \cdot (\mathbf{f}_c - \mathbf{f})\right]^{3/2}, \tag{4}$$

where $\nabla\nabla\nabla U(\mathbf{x}_c)$ is the third-order gradient tensor of U at $\mathbf{x}_c$, and λ is the relative spring stiffness tensor given in the Supplemental Material [16]. Figure 2(b) shows ΔV as a function of $\mathbf{f}$ in the 2D force space for the same energy landscape as in Fig. 2(a). Following the Kramers' rate theory [20], Ω^2 should

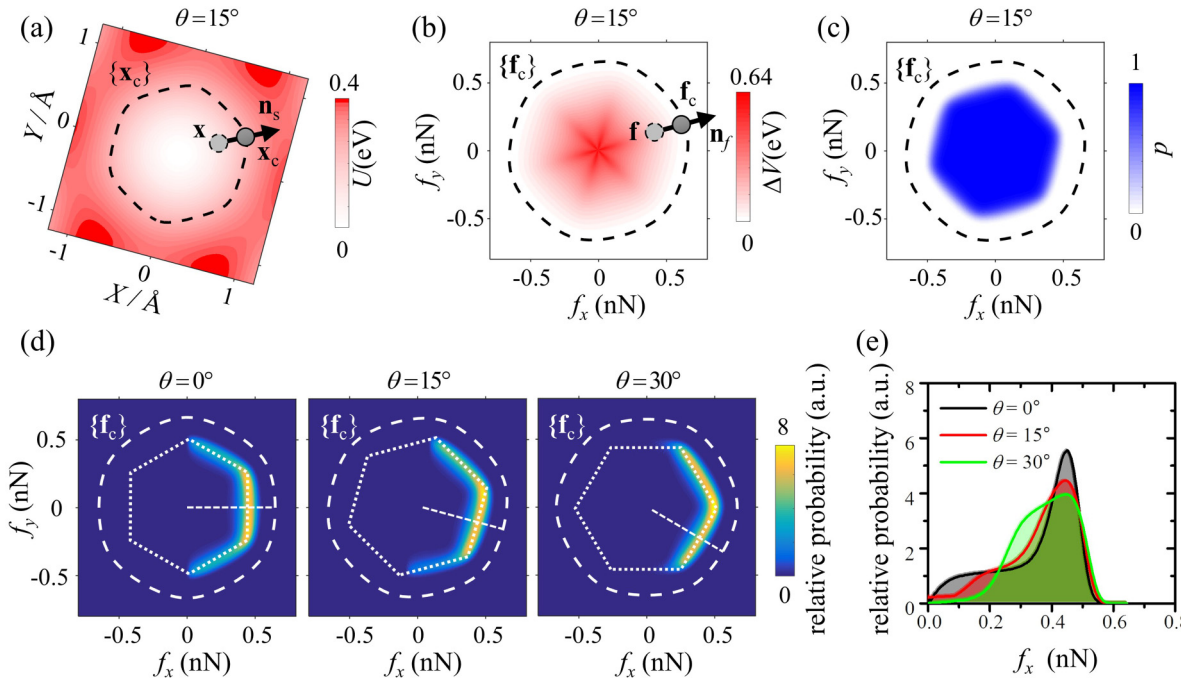

FIG. 2. (a) Zoom-in view of the energy landscape near a minimum point. The dashed curve represents $\{\mathbf{x}_c\}$. (b) A contour plot showing the energy barrier V as a function of $\mathbf{f}$ calculated by Eq. (1). The dashed curve represents $\{\mathbf{f}_c\}$. (c) A contour plot showing the probability p, at which a slip does not occur. The dashed curve represents $\{\mathbf{f}_c\}$. (d) 2D histogram of slip forces for $\theta = 0°$ (left panel), $\theta = 15°$(middle panel) and $\theta = 30°$(right panel). The dashed curves represent $\{\mathbf{f}_c\}$ and the dotted lines are guidelines to visually show the trend. (e) 1D histograms of slip force f_x if all slip events in (d) are counted.

take the following form:

$$\Omega^2 = \frac{\sqrt{2}}{m}\left[-\mathbf{n}_s\mathbf{n}_s\mathbf{n}_s \vdots \nabla\nabla\nabla U(\mathbf{x}_c)\right]^{1/2} \times [\mathbf{n}_s \cdot (\mathbf{I}+\lambda) \cdot (\mathbf{f}_c - \mathbf{f})]^{1/2}. \quad (5)$$

Therefore, the probability, p, at which a transition has not yet occurred, can be determined by the master equation:

$$dp/dt = -\kappa p, \quad (6)$$

whose left-hand side can be rewritten as

$$\frac{dp}{dt} = \frac{\partial p}{\partial f_x}\frac{\partial f_x}{\partial s_x}\frac{ds_x}{dt} = k_{\text{eff}} v \frac{\partial p}{\partial f_x}, \quad (7)$$

where k_{eff} is the composite stiffness in the x direction and v is the speed of the support (See more details in the Supplemental Material [16]). It should be noted that in Eq. (5), the backward slips are neglected, which holds only when the backward slip energy barrier is much larger than the forward slip one. From Eqs. (3)–(7), we can obtain the general solution for the probability $p(\mathbf{f})$ as follows:

$$p(\mathbf{f}) = \exp\left[-\frac{1}{v^*}\exp\left(-\frac{\Delta V}{k_B T}\right)\right]. \quad (8)$$

In Eq. (8), v^* is the dimensionless velocity given by

$$v^* = \cos(\mathbf{n}_f)\frac{4\pi m\gamma v k_{\text{eff}}}{k_B T}[-\mathbf{n}_s\mathbf{n}_s\mathbf{n}_s \vdots \nabla\nabla\nabla U(\mathbf{x}_c)]^{-1} \times [\mathbf{n}_s \cdot (\mathbf{I}+\lambda) \cdot \mathbf{n}_f], \quad (9)$$

where $\mathbf{n}_f$ is a unit vector defined by

$$\mathbf{n}_f \Delta f = \mathbf{f}_c - \mathbf{f}. \quad (10)$$

Theoretically, in the above equation, one needs to find the critical force vector f_c that is "nearest" to $\mathbf{f}$ in the 2D force space, which can be done numerically if the specific shape of the energy landscape is known (see more details in the Supplemental Material [16]). However, for energy landscape (e.g., hexagonal shape) with weak directional anisotropy, one can simply choose the critical force vector f_c that is parallel to $\mathbf{f}$.

Figure 2(c) shows p as a function of $\mathbf{f}$ in the 2D force space calculated from the same system parameters used for Fig. 1. Based on the distribution of p, the probability density of transition (i.e., slip) as a function of $\mathbf{f}$ can be readily obtained by $P = -dp/df_x$, which are shown by the 2D histograms of slip forces in Fig. 2(d). Comparing Fig. 2(d) with Fig. 1(e), one can see that the theoretical predictions show reasonable consistency with the 2D Langevin simulation results for all three sliding angles. As visually indicated by the dotted curves in Fig. 2(d), the contour of the local most-probable slip forces appears to form a partial hexagonal annulus for all three cases, which is expected since both the energy corrugation and its gradients exhibit rotational symmetry with a period of 60°. Because of the 2D nature of the slip force distribution, variation of P with f_x would depend sensitively on the value of f_y, which also suggested the 2D fluctuations of the tip apex is providing extra help for the tip to slip forward. If one blindly counts all the slip events regardless the value of f_y, the resultant distribution will be messed up and exhibits

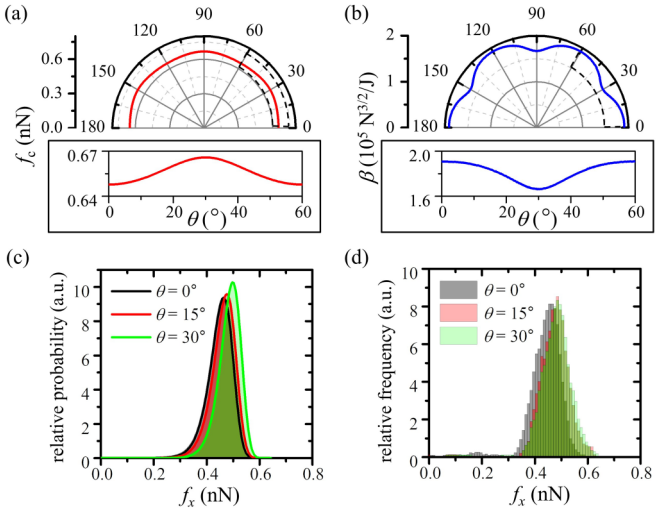

FIG. 3. (a) Reduced critical slip force f_c as a function of θ when $f_y = 0$. The lower panel shows an enlarged view between 0 to 60°. (b) Energy corrugation shape factor β as a function of θ when $f_y = 0$. The lower panel shows an enlarged view between 0 to 60°. (c) Reduced histograms of f_x when $f_y = 0$ for $\theta = 0°$ (black), $\theta = 15°$(red) and $\theta = 30°$(green) from 2D theoretical prediction. (d) Reduced histograms of f_x when slip events with f_y in the range of 0 ± 0.01nN for $\theta = 0°$(black), $\theta = 15°$(red) and $\theta = 30°$(green) from 2D Langevin simulation.

a complicated dependence on sliding angle θ, as shown in Figs. 2(e) and 1(d).

Theoretically, Eq. (8) provides a possible means of extracting the interfacial parameters using the 2D slip force distribution from experiments. However, direct fitting using Eq. (8) would be mathematically cumbersome due to the complicated and nonlinear tensor calculation involved. However, according to our previous derivation, if one only chooses slip events with a specific value of f_y, say $f_y = 0$, then for these slip events ΔV will be reduced to $\Delta V = \frac{1}{\beta}[f_c - f_x]^{3/2}$, where $\beta = \frac{3\sqrt{2}}{8}[-\mathbf{n}_s\mathbf{n}_s\mathbf{n}_s \vdots \nabla\nabla\nabla U(\mathbf{x}_c)]^{1/2}[\mathbf{n}_s \cdot (\mathbf{I} + \lambda) \cdot \mathbf{n}_f]^{-3/2}$ and f_c is the x component of the corresponding $\mathbf{f}_c$ whose y component is zero (see the Supplemental Material [16] for details). This reduced form coincides exactly with the 1D expression originally introduced by Sang *et al.* [6]; however it should be noted that the reduced f_c and β are dependent on θ. For the specific system we explored, variations of f_c and β are only about 5% and 15% respectively as shown in Figs. 3(a) and 3(b). Consequently, the reduced distribution of f_x when $f_y = 0$ should also be insensitive to θ, which is confirmed by our model calculation [Fig. 3(c)] as well as the 2D Langevin simulation [Fig. 3(d)]. Although this weak angular dependence of f_c and β is numerically demonstrated for the specific systems we adopted, we expect it to be valid for other systems with hexagonal energy landscapes (or energy landscapes with weak anisotropy) and a relatively compliant spring. Based on the above analysis, we propose that, by identifying the slip events with $f_y \sim 0$, one can obtain a reduced slip force distribution that can be approximately described or fitted using the traditional 1D PTT model. It should be noted that this approach does not require scanning along the close-packed direction as in previous work [3] and it can be applied to schemes with arbitrary scan angle.

To further validate the 2D theoretical model, we conducted atomic stick-slip friction measurement on a freshly cleaved Bi_2Se_3, a layer-structured crystal with a hexagonal lattice, in ambient conditions. As schematically shown in Fig. 4(a),

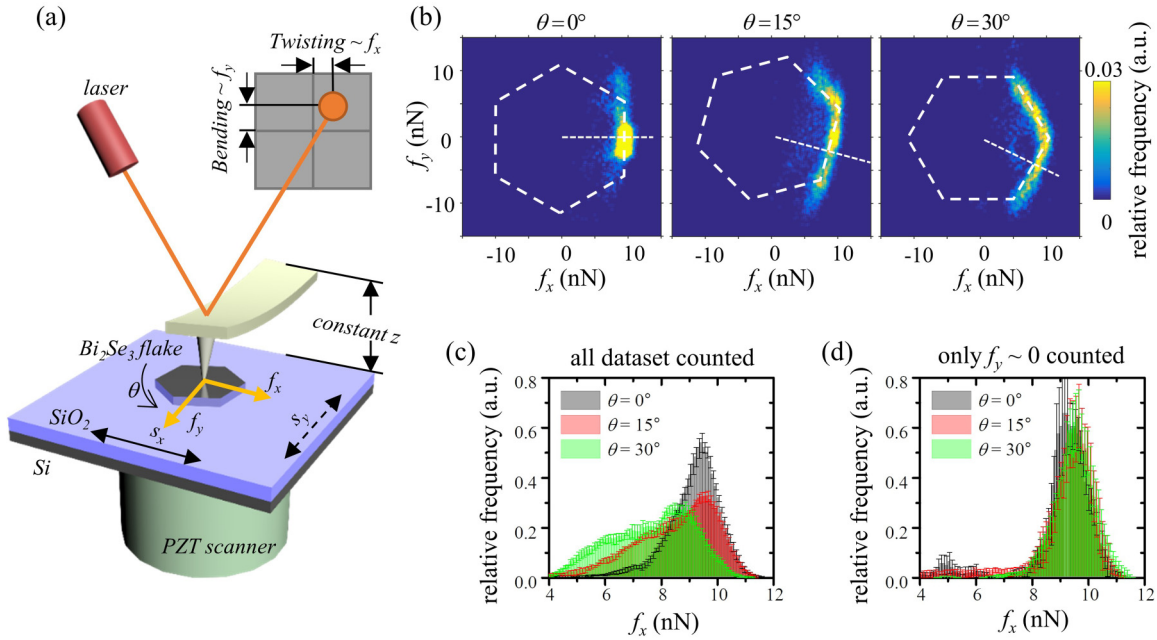

FIG. 4. (a) A schematic showing the experimental setup. (b) 2D slip force histograms for $\theta = 0°$(left panel), $\theta = 15°$(middle panel) and $\theta = 30°$(right panel). The dashed lines are guidelines to visually highlight the trends. (c) Histograms of slip force f_x for $\theta = 0°$(black), $\theta = 15°$(red) and $\theta = 30°$(green) when all slip events are counted. (d) Reduced histograms of f_x when slip events with f_y in the range of 0 ± 0.1nN for $\theta = 0°$(black), $\theta = 15°$(red) and $\theta = 30°$(green).

we adopted constant-height mode and measured the real-time torsional and bending signals of the cantilever [27], which were then calibrated to represent f_x and f_y, respectively (see the Supplemental Material [16]). We also carefully rotated the sample to change the angle between the scanning direction and the close-packed direction of the Bi_2Se_3 lattice for $\theta = 0^\circ, 15^\circ, 30^\circ$. Apparently different patterns of stick-slip motion were observed on the two force channels when the scan direction was varied (see the Supplemental Material [16] for more information). Then we extracted the slip force using the modified LSR method [11] and plotted the 2D slip force histograms for $\theta = 0^\circ, 15^\circ, 30^\circ$.

As shown in in Fig. 4(b), the hexagonal annulus shape of the 2D slip force distributions and the rotational characteristics are qualitatively consistent with the trend predicted by the 2D theoretical model. As expected, if we blindly counted all the slip events, the traditional accumulated 1D slip force distribution would be irregular and differ significantly for different scan angles, as shown in Fig. 4(c). However, if we only consider the slip events with $f_y \sim 0$ (i.e., $f_y < 1/100 \cdot \mathrm{Max}(|f_c|)$), the reduced slip force distributions are almost overlapping even when the scan angle is varied, as shown in Fig. 4(d). From the reduced 1D slip force distributions, we could more consistently extract the interfacial parameters by fitting the traditional 1D PTT model (see more details in the Supplemental Material [16]). Therefore, the experiment directly validates the 2D theoretical model and confirms that the reduced slip force distribution from 2D experiments indeed matches well with the 1D PTT model.

To conclude, we have shown both experimentally and numerically that the slip statistics of the widely observed atomic stick-slip friction exhibits an intrinsically 2D nature, which usually cannot be captured by traditional 1D model. Based on the framework of transition state theory, a 2D slip model considering thermal activation effect is proposed and a 2D slip force histogram is obtained theoretically. The theoretical predictions have been validated by atomic stick-slip friction experiment on crystalline surface with a hexagonal lattice. The rich features revealed by the 2D model highlight the need to study atomic process of friction with higher dimensionality.

We gratefully acknowledge the support from the National Natural Science Foundation of China (12025203, 11772169, 11890671 and 11921002), and the State Key Laboratory of Tribology at Tsinghua University (Grant No. SKLT2022A01).

[1] C. M. Mate, G. M. McClelland, R. Erlandsson, and S. Chiang, Phys. Rev. Lett. **59**, 1942 (1987).
[2] Q. Li, Y. Dong, D. Perez, A. Martini, and R. W. Carpick, Phys. Rev. Lett. **106**, 126101 (2011).
[3] A. Schirmeisen, L. Jansen, and H. Fuchs, Phys. Rev. B **71**, 245403 (2005).
[4] L. Prandtl, ZAMM-J. Appl. Math. M./Z. Angew. Math. Mech. **8**, 85 (1928).
[5] G. Tomlinson, Lond. Edinb. Dublin Philos. Mag. J. Sci. **7**, 905 (1929).
[6] Y. Sang, M. Dubé, and M. Grant, Phys. Rev. Lett. **87**, 174301 (2001).
[7] E. Riedo and E. Gnecco, Nanotechnology **15**, S288 (2004).
[8] M. H. Müser, Phys. Rev. B **84**, 125419 (2011).
[9] X. Z. Liu, Z. Ye, Y. Dong, P. Egberts, R. W. Carpick, and A. Martini, Phys. Rev. Lett. **114**, 146102 (2015).
[10] L. Jansen, H. Holscher, H. Fuchs, and A. Schirmeisen, Phys. Rev. Lett. **104**, 256101 (2010).
[11] Q. Yao and Q. Li, Tribol. Lett. **64**, 31 (2016).
[12] S. Morita, S. Fujisawa, and Y. Sugawara, Surf. Sci. Rep. **23**, 1 (1996).
[13] O. E. Dagdeviren, Nanotechnology **29**, 315704 (2018).
[14] Y. Dong, A. Vadakkepatt, and A. Martini, Tribol. Lett. **44**, 367 (2011).
[15] O. Y. Fajardo, E. Gnecco, and J. J. Mazo, Physica B **455**, 44 (2014).
[16] See Supplemental Material at http://link.aps.org/supplemental/10.1103/PhysRevB.105.165429 for simulation method, data processing with the LSR method, derivation of the 2D theoretical model, theoretical prediction from traditional 1D model, instrument setup and data processing in experiments, which includes Refs. [3,6,11,14,17–21].
[17] T. Gyalog, M. Bammerlin, R. Lüthi, E. Meyer, and H. Thomas, EPL (Europhys. Lett.) **31**, 269 (1995).
[18] P. Steiner, R. Roth, E. Gnecco, A. Baratoff, S. Maier, T. Glatzel, and E. Meyer, Phys. Rev. B **79**, 045414 (2009).
[19] Y. Dong, D. Perez, H. Gao, and A. Martini, J. Phys.: Condens. Matter **24**, 265001 (2012).
[20] P. Hänggi and M. Borkovec, Rev. Mod. Phys. **62**, 251 (1990).
[21] Q. Li, K. S. Kim, and A. Rydberg, Rev. Sci. Instrum. **77**, 065105 (2006).
[22] Y. Sang, M. Dubé, and M. Grant, Phys. Rev. E **77**, 036123 (2008).
[23] M. Evstigneev and P. Reimann, Phys. Rev. B **87**, 205441 (2013).
[24] S. Medyanik, W. Liu, I.-H. Sung, and R. Carpick, Phys. Rev. Lett. **97**, 136106 (2006).
[25] E. Riedo, E. Gnecco, R. Bennewitz, E. Meyer, and H. Brune, Phys. Rev. Lett. **91**, 084502 (2003).
[26] E. Gnecco, R. Bennewitz, T. Gyalog, C. Loppacher, M. Bammerlin, E. Meyer, and H.-J. Güntherodt, Phys. Rev. Lett. **84**, 1172 (2000).
[27] S. G. Balakrishna, A. S. de Wijn, and R. Bennewitz, Phys. Rev. B **89**, 245440 (2014).